Deep–Sea Research II 219 (2025) 105450

Contents lists available at ScienceDirect

Deep-Sea Research Part II

journal homepage: www.elsevier.com/locate/dsr2

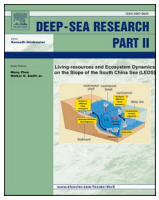

The relative contribution of deep and shallow benthic sources to iron supply in the Ross sea, with specific emphasis on Ross Bank

Blair J.W. Greenan [a,*], Michael S. Dinniman [b], Dennis J. McGillicuddy Jr. [c], Peter N. Sedwick [b], Stefanie L. Mack [d], Walker O. Smith Jr. [e,f]

[a] Bedford Institute of Oceanography, Fisheries and Oceans Canada, Dartmouth, NS, B2Y 4A2, Canada
[b] Department of Ocean and Earth Sciences, Old Dominion University, Norfolk, VA, 23529, USA
[c] Woods Hole Oceanographic Institution, Woods Hole, MA, 02543, USA
[d] Center for Global Education, University of Tokyo, Tokyo, Japan
[e] Virginia Institute of Marine Science, College of William and Mary, Gloucester Point, VA, 23062, USA
[f] School of Oceanography, Shanghai Jiao Tong University, Shanghai, China

ARTICLE INFO

Handling Editor: Prof. J Aristegui

Keywords:
Ross sea
Benthic iron supply

ABSTRACT

Summer primary productivity in the Ross Sea is limited by the availability of dissolved iron (DFe) in the euphotic zone. Previous studies have suggested that benthic sources dominate the supply of DFe to the upper water column in the southern Ross Sea polynya. The purpose of this study is to investigate whether these benthic sources are derived from shallow banks or deeper areas of the continental shelf. Our study combines analysis of *in situ* observations near Ross Bank with a physical ocean model simulation in an overlapping summertime period to investigate the vertical supply of DFe. Two passive tracer dyes were employed in the ocean model with the first (second) being input in the bottom model layer over seabed depths of less (greater) than 400 m. The tracer dyes provide temporal (March 2011–January 2012) and spatial estimates of the advection, mixing and diffusion throughout the Ross Sea model domain, and enable estimates of the relative contributions of shallow and deep benthic iron sources to the upper ocean DFe inventory. A comparison of the model output with a ship-based survey and a mooring deployed on Ross Bank in January 2012 provides confidence that the model simulations produce a sufficiently accurate representation of ocean conditions to support estimates of benthic DFe supply to surface waters. The results demonstrate that for Ross Bank the local (on-bank) benthic supply is important during the early winter period, whereas for most of the year the deep (off-bank) benthic iron is the predominant source supplying the upper ocean over this shallow region.

1. Introduction

The Southern Ocean is the largest high nutrient, low chlorophyll (HNLC) region in the world ocean (Martin, 1990) and this state is attributed to the low availability of dissolved iron (DFe), a micronutrient essential for phytoplankton growth. Satellite studies show that typical HNLC chlorophyll *a* concentrations (Chl a) of <0.5 mg m^{-3} are found in ice-free surface waters around Antarctica (Arrigo et al., 2008; Fitch and Moore, 2007). However, there are exceptions to these low chlorophyll conditions, and areas with much higher Chl a ($\sim$2–20 mg m^{-3}) are found around islands and in coastal and shelf sea regions (Arrigo et al., 1998; Moore and Abbott, 2000). One such region is the Ross Sea continental shelf, which is among the most productive areas of the Antarctic continental margin (Arrigo et al., 2008; Smith et al., 2014). Iron limitation of phytoplankton growth has been demonstrated in field studies of the Ross Sea during the austral summer growing season (Bertrand et al., 2007; Coale et al., 2003; Martin et al., 1991; Sedwick et al., 2000, 2011; Sedwick and DiTullio, 1997).

Mechanisms that may supply DFe and particulate Fe to surface waters of the Ross Sea include circumpolar deep water (CDW) intrusions from the shelf edge (Castagno et al., 2017; Kohut et al., 2013), sediments from shallow banks and coastal areas, sea ice meltwater from the perimeter of the polynya and glacial meltwater from the Ross Ice Shelf (Sedwick et al., 2011). The relative importance of these supply processes depends both on the time of the year and the location in the Ross Sea (Kustka et al., 2015; Mack et al., 2017; McGillicuddy et al., 2015;

* Corresponding author.
E-mail address: blair.greenan@dfo-mpo.gc.ca (B.J.W. Greenan).

https://doi.org/10.1016/j.dsr2.2024.105450
Received 28 March 2024; Received in revised form 15 December 2024; Accepted 22 December 2024
Available online 27 December 2024

Salmon et al., 2020; Sedwick et al., 2022). The complex interaction of the physical environment and phytoplankton dynamics results in a strong seasonal cycle of DFe in the surface waters, with DFe exhibiting a nutrient-like distribution during the summer months, when it is drawn down to growth-limiting concentrations of ~0.1 nM in the upper water column. In addition to release of DFe from remineralization of organic matter below the euphotic zone, DFe is also scavenged by sinking and suspended particles (Boyd and Ellwood, 2010; Tagliabue et al., 2019). This leads to a vertical decoupling of DFe from macronutrients, such that the ferricline is observed to be substantially deeper than the nutricline over the Ross Sea continental shelf during the growing season (Fitzwater et al., 2000; Sedwick et al., 2011; Smith et al., 2006).

It has been inferred that the vertical resupply of DFe occurs primarily during the winter months when sea ice formation and deep convective mixing are the dominant physical processes in the coastal polynyas of the Ross Sea (Marsay et al., 2014; McGillicuddy et al., 2015; Sedwick et al., 2011). Recent observations in late austral fall suggest that the timing of the resupply is mainly in mid-late winter, and that this process is sensitive to changes in the timing and extent of sea ice production (Sedwick et al., 2022). The low productivity period typically ends abruptly with the onset of the spring bloom and rapid drawdown of nutrients and DFe (Sedwick et al., 2011). After net primary productivity peaks in late December, it remains high through the summer (Smith and Kaufman, 2018), even though the DFe concentrations in the euphotic zone remain low (<0.1 nM) during that period (Sedwick et al., 2011). The primary production through the summer period may be sustained through recycling of particulate Fe in the upper water column (Marsay et al., 2017). It is also possible that a vertical flux of DFe from deeper water into the euphotic zone could occur during summer (Gerringa et al., 2015), although the strong stratification that occurs throughout the summer in the Ross Sea should limit the extent of vertical mixing.

In the Ross Sea, diatoms grow after Phaeocystis biomass is reduced (likely because of increased losses due to Fe stress), and while chlorophyll increases modestly, particulate organic carbon increases markedly, resulting in an elevated carbon/chlorophyll ratio. This is seen in the climatology as well as in satellite estimates of chlorophyll and particulate organic carbon (Chen et al., 2021). While there are multiple potential acclimations to low Fe, it seems likely that phytoplankton in the Ross Sea acclimate to the low DFe environment by reducing chlorophyll synthesis but maintaining carbon fixation, resulting in elevated particulate organic carbon to chlorophyll ratios (Smith and Kaufman, 2018).

In this context, elevated DFe concentrations observed in the water column over shallow bathymetry in the Ross Sea suggest that accumulation and remineralization of organic matter on submarine banks may facilitate the vertical resupply of DFe to the euphotic zone throughout the year (Gerringa et al., 2015; Marsay et al., 2014). Moreover, vertical DFe fluxes have been estimated to be high above submarine banks and slopes due to a combination of a smaller distance from the benthic DFe source and enhanced eddy diffusivity (Gerringa et al., 2015). Ocean model results indicate that blooms are supported by enhanced vertical supply over shallow banks (Salmon et al., 2020) that contribute up to 50% of the total DFe (Mack et al., 2017). These results are further supported by phytoplankton incubation experiments conducted in the Ross Bank region during summer showing no significant response to iron addition, which suggests that this shallow bank may provide significant and continuous DFe inputs to the euphotic zone (Ryan-Keogh et al., 2017). Observations and modeling of DFe above the Ross, Pennell and Mawson banks demonstrate that the physical mechanisms controlling this vertical supply do differ with location over the Ross Sea shelf (Gerringa et al., 2015; Kohut et al., 2017; Kustka et al., 2015; Mack et al., 2017).

In the austral summer, the lowest dFe concentrations in the Ross Sea are generally found in the upper 50 m of the water column. In areas of relatively shallow bathymetry (<400 m), mid-depth DFe concentrations (100–300 m interval) are often elevated relative to the same interval in deeper areas of the shelf (Marsay et al., 2014). In these shallow bathymetry areas, DFe concentrations increase approximately linearly with depth until reaching a near constant value (generally <0.3 nM) in a layer several tens of meters above the seabed (Marsay et al., 2014). In contrast, the profiles of DFe over deeper locations (>400 m) exhibit a quasi-exponential increase in concentration where values within 50 m of the seabed have an average of 0.74 ± 0.47 nM (Marsay et al., 2014). The differences observed in benthic DFe concentrations in shallow and deep locations are consistent with the distribution of seafloor sediments, which are characterized by coarse glacial-marine sediments over banks and shoals, and siliceous muds and oozes in the deeper areas (Anderson, 1999; Barry et al., 2003; Dunbar et al., 1985). The near-bottom sediments in the shallower areas are expected to contain a smaller proportion of organic matter and hence conditions that are less effective at reducing and releasing iron into pore waters and overlying bottom waters.

While previous studies have suggested that benthic sources dominate the supply of DFe to the upper water column in the southern Ross Sea polynya, little remains known about which benthic areas of the continental shelf are most important for this source. The purpose of this study is to provide new insights into the relative role of deep versus shallow benthic sources in the vertical supply of dFe over shallow banks in the Ross Sea. This study employs ship-based and moored field data collected over Ross Bank in combination with a numerical ocean model. This approach leverages the insights from *in situ* data to support the model run which extends for a period beyond the field survey.

2. Methods

2.1. Field observations

The field observations were collected as part of the project *Processes Regulating Iron Supply at the Mesoscale - Ross Sea* (PRISM-RS). This work was carried out on voyage NBP12-01 of the RVIB *Nathaniel B. Palmer* during the austral summer period of December 24, 2011 to February 8, 2012. To support the objective of this paper, we focus on the Ross Bank region in which multiple platforms were used to collect data during the period of 19–26 January 2012 (Fig. 1).

2.1.1. Hydrography and water samples

Hydrographic data were collected with a Sea-Bird SBE 911plus CTD instrument package, with dual temperature, conductivity and oxygen sensors. Additional auxiliary sensors on the CTD system included a Wet Labs ECO-AFL/FL fluorometer, SeaTech transmissometer, and Biospherical QSP-200L4S photosynthetically available radiation (PAR) sensor. Water samples were collected from the CTD rosette system, comprised of 24 10-L Niskin bottles, for chlorophyll and macronutrient measurements.

The CTD survey of Ross Bank was comprised of two occupations: 20–22 January 2012 (casts 37–57) and January 26, 2012 (casts 74–80) shown in Fig. 1. The other Ross Bank sections occupied during this study are presented in Figs. S2 and S3. The CTD salinity, oxygen and chlorophyll fluorescence data were calibrated after the cruise using discrete bottle samples from the rosette for calibration, which were processed using standard GO-SHIP protocols (https://www.go-ship.org/HydroMan.html).

2.1.2. Trace metal sampling

Water column samples for trace element analysis were collected at six casts over Ross Bank (Fig. 1) using Teflon-lined 5-L Niskin-X samplers (General Oceanics) that were custom-modified for trace metal sampling and deployed on a trace-metal clean CTD carousel unit (Sea-Bird Electronics) using a Kevlar line (Marsay et al., 2014). In addition, near-surface water samples (~3 m depth) were collected while underway using a trace-metal clean towfish system, as described by Sedwick et al. (2011). Five of the casts (TM26-30) were collected during the first

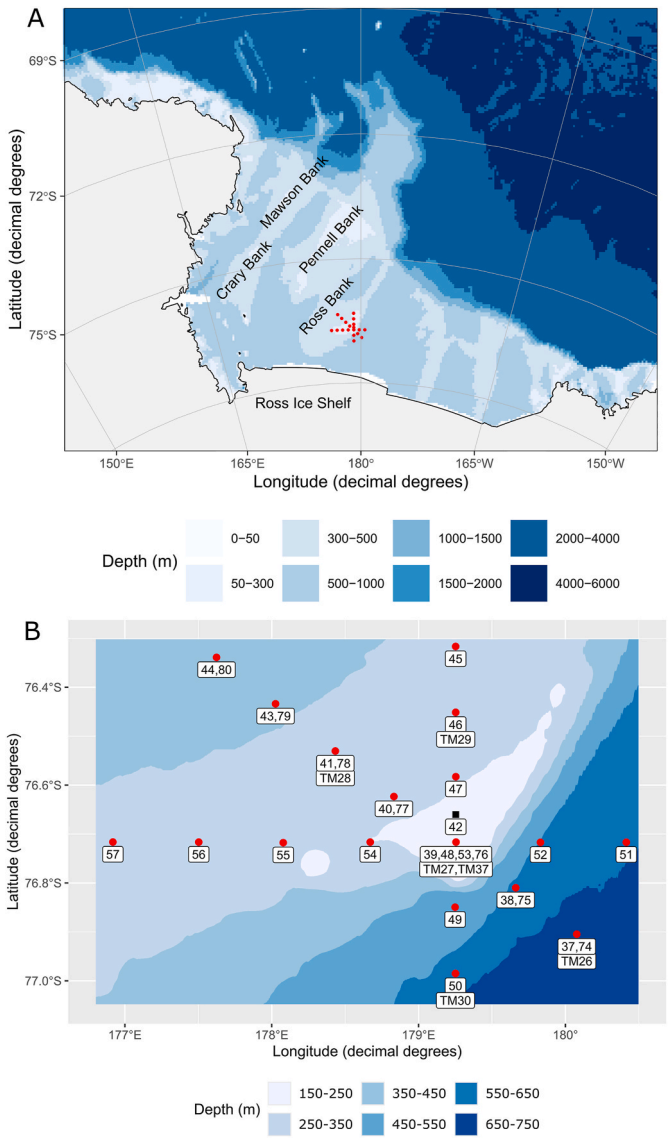

Fig. 1. A) Map of the Ross Sea including the Ross Bank CTD station locations (red circles). B) CTD stations occupied during the two surveys of Ross Bank (red circles) labeled with the cast number for the CTD (number only) and Trace Metal CTD (TM prefix). The black square represents the location of the SeaHorse mooring. (For interpretation of the references to color in this figure legend, the reader is referred to the Web version of this article.)

occupation of Ross Bank, and one cast (TM37) was collected on the second survey. Casts TM27 and TM37 were taken at the same location on the crest of Ross Bank.

Dissolved iron was determined in 0.2-μm filtered, acidified water-column (pH 1.7) and near-surface samples at Old Dominion University using flow-injection analysis with in-line preconcentration of on resin-immobilized 8-hydoxyquinoline followed by spectrophotometric detection modified from the method of Measures et al. (1995). Determinations of DFe concentrations in SAFe seawater reference materials S and D2 using this method were in good agreement with consensus values. Based on previous multiple separate analyses of seawater consensus reference materials SAFe S1 and SAFe D2, overall analytical uncertainty is estimated to be less than ±10%, expressed as ± one relative standard deviation on the mean (Sedwick et al., 2011). A more detailed description of the water sample processing and analysis is provided by Marsay et al. (2017, 2014).

2.1.3. Vessel-mounted ADCP

Vessel-mounted acoustic Doppler current profiler (VM-ADCP) data were acquired using a Teledyne RD Instruments 150-kHz narrowband instrument (NB150). The NB150 collects profiles with an 8-m vertical resolution and can provide data to a depth of ~350 m. The transducer depth was 7 m with a blanking length of 16 m. The system was operated with bottom track mode enabled and an ensemble averaging period of 300 s. The UHDAS (University of Hawaii Data Acquisition System) acquired data from NB150 and ancillary sensors and processed the data in real-time to support survey planning.

2.1.4. Ross Bank mooring

A mooring was deployed on Ross Bank (76° 39.60′ S, 179° 15.20’ E, water depth 223 m) from 21 to 26 January 2012 to provide data near the crest of the bank during both CTD surveys, and the period in between. The mooring included two RDI Workhorse 300 kHz broadband ADCPs at water depths of 5 m (downward-looking) and 210 m (upward-looking, see Fig. S1). The ADCPs collected a 5-min sample every hour in 4-m depth bins with an approximate range of 100 m from the instruments.

The SeaHorse profiler (Greenan et al., 2008; Hamilton et al., 1999) collected data in the water column between the two ADCPs. SeaHorse is a positively buoyant platform that uses surface wave energy and a one-way clamping mechanism to enable it to descend along the mooring wire until it reached a docking position at about 210 m depth. It remained in the docking position until a pre-set time interval elapsed, at which point the clamp on the mooring wire was released and the SeaHorse ascended smoothly to the surface at ~0.5 m s^{-1} while collecting measurements. The SeaHorse cycled between 5 and 210 m every hour. The payload for this field program included a Sea-Bird SBE19plus CTD (sampling rate 4 Hz) with an SBE43 oxygen sensor, WETLabs WETStar fluorometer and Satlantic OCR-504i multispectral radiometer (four wavelengths at 380, 440, 490 and 555 nm). The CTD, oxygen and fluorometer data were processed into 1-m vertical bins using standard protocols with Sea-Bird processing software and factory calibrations from the manufacturers.

If the SeaHorse profiler was in the sampling range of the ADCP, this would create sidelobe interference in the acoustic return signal. To minimize any potential sidelobe issue, the downward-looking ADCP (at 5 m depth) was programmed to collect a velocity sample for 5 min before the top of the hour. During this sampling period, the SeaHorse profiler was clamped at the bottom of the mooring wire at 210 m. At the top of each hour, the SeaHorse released its clamp and began its ascent along the mooring wire, which required about 6 min to complete. At 5 min after the top of the hour, the upward-looking ADCP (at 210 m) started sampling for a 5-min period. During this period the SeaHorse profiler had ascended far enough along the mooring wire that it was beyond the range of the ADCP.

2.1.5. Satellite ocean color

Data from the MODIS Aqua satellite (Level-3 data) with a spatial resolution of ~4 km were obtained from the NASA Goddard Space Flight Center (http://oceancolor.gsfc.nasa.gov/). All data were reprocessed using the algorithms described by Chen et al. (2021), which have a greater correlation with observations than previous analyses.

2.2. Model simulations

The Ross Sea circulation model used in this study is based on the Regional Ocean Modeling System (ROMS v3.6) framework with vertical terrain-following levels (Haidvogel et al., 2008; Shchepetkin and McWilliams, 2005, 2009). The domain of the model includes the Ross Sea continental shelf and shelf break region, as well as the Ross Ice Shelf cavity (see Fig. 1, Mack et al., 2017).This model (Dinniman et al., 2007, 2011; Mack et al., 2017; McGillicuddy et al., 2015) includes the Ross Ice Shelf cavity, thermodynamic and mechanical effects of the ice shelf on the ocean, and a coupled dynamic sea ice model (Budgell, 2005). The

bathymetry products used (Arndt et al., 2013; Fretwell et al., 2013) were smoothed to eliminate pressure gradient force errors in the regions with steep gradients in bathymetry or topography relative to total depth. The model setup employed a vertical stretching scheme (Song and Haidvogel, 1994) with 24 levels, allowing for enhanced resolution near the ocean surface and the seafloor. For example, this resulted in on-shelf locations in the model with a depth of 500 m having 5 m thick layers near the surface, 38 m thick layers at mid-depth and 12 m thick layers near the seafloor.

Hindcast simulations for the period of Sep 2010 to Feb 2012 begin with a 6-year spin up (Dinniman et al., 2011), which was forced with a 2-year repeating cycle of daily winds from Antarctic Mesoscale Prediction System (AMPS) (Powers et al., 2003), monthly AMPS climatologies of humidity, sea level pressure, air temperature and precipitation, and cloud cover from the International Satellite Cloud Climatology Product (ISCCP) (Rossow et al., 1996). The spin up allows the model simulation to start from a stable configuration with established flow patterns and temperature/salinity fields. With a 1.5 year simulation, we allowed the model to adjust to the 2010–2012 forcing for six months before using the output for analysis (i.e., the model results presented cover the period of March 2011 to January 2012 with the last month overlapping the PRISM-RS field survey).

During the 1.5 year simulation, the model is forced with 6-hourly winds and air temperature and monthly climatologies of humidity, precipitation and cloud cover from the ERA-Interim reanalysis (Dee et al., 2011). The open boundary conditions for the simulation were provided by monthly sea ice concentration from SSM/I data (Cavalieri et al., 1996), monthly climatologies of ocean temperature and salinity from the World Ocean Atlas (Boyer et al., 2018), and monthly non-tidal barotropic velocities from the Ocean Circulation and Climate Advanced Model (OCCAM) (Saunders et al., 1999). Lateral open boundary conditions specify a radiation scheme on outflow, and a weak nudging on inflow. Vertical mixing of tracers and momentum is estimated using the K-profile parameterization scheme (Large et al., 1994) along with a bottom boundary layer parameterization (Durski et al., 2004).

The model simulation included forcing with tidal constituents O1, K1, M2 and S2, which are added at the boundaries as both sea surface height and velocity. The amplitude and phase of the tidal constituents were derived from the CATS2008 tidal model (Padman et al., 2002) and were nodally corrected. The ROMS model was run with an eddy-resolving resolution of 1.5 km (Mack et al., 2017) and, other than the passive tracer dyes mentioned below, the model was the same as the 1T simulation in that paper.

The ocean model included two conservative passive tracer dyes, both of which were added as a proxy for benthic iron sources, including sediment efflux and benthic remineralization. The first (second) tracer dye is seeded in the bottom model layer for all locations over the continental shelf with a water depth of less than (greater than) 400 m. For this simulation, the extent of the continental shelf is defined by locations inshore of the 700 m isobath that are not beneath an ice shelf. The intention of this two-tracer dye scheme is to assess the relative importance of shallow and deep benthic sources of DFe to the water column of the Ross Sea. Each tracer dye is ramped in during the month prior to March 15, 2011, and is fully set in the bottom boundary layer at that date. The choice to start this process in March is based on the assumption that the phytoplankton bloom had ended and the surface DFe was correspondingly low, hence the system was closest to the point of "seasonal reset" in terms of vertical resupply of DFe. The concentration of the tracer dye in the bottom model layer is maintained with a constant value (set as 100) throughout the model run, allowing transport to be determined by advection, mixing and turbulent diffusion. To account for the observed difference in DFe concentration in the shallow and deep regions, the tracer dye in this analysis will be converted using end member DFe concentrations of 0.4 and 1.5 nM, respectively (see Fig. 2, Marsay et al., 2014). The choice of these end-member DFe concentrations included consideration that the *in situ* CTD sampling did not get closer than 10 m from the seafloor while the bottom layer thickness of the ocean model is approximately 10 m in the deep regions and less over the shallow banks. Therefore, we believe that the DFe concentrations in the bottom model layer should be slightly larger than those observed at the deepest CTD sample depths. It is important to note that the ROMS model employing such tracer dyes can only provide insights into the physical processes that contribute to the availability of DFe in the water column over Ross Bank; the model does not account for chemical (e.g., scavenging or precipitation) or biological processes (e.g., assimilation or remineralization) that affect DFe concentrations.

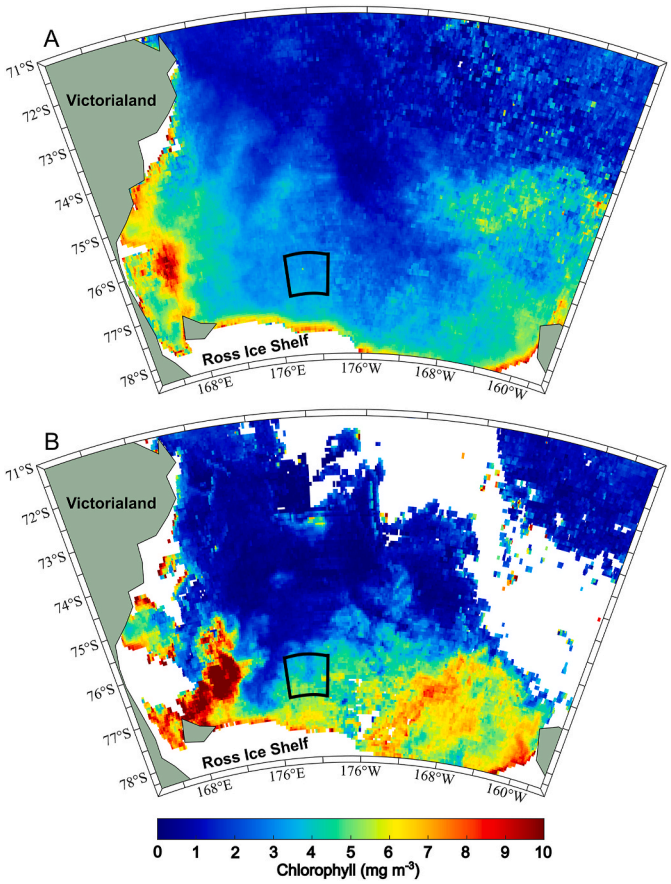

Fig. 2. A) Satellite-derived chlorophyll climatology for the Ross Sea over the month of January for the period of 2002–2020 and B) January 2012. The black box represents the Ross Bank CTD survey area shown in Fig. 1.

3. Results

3.1. Ocean color

Satellite imagery from the austral summer shows chlorophyll concentrations in January 2012 that were substantially higher than the climatological average for the area south of 75°S (Fig. 2). There is significant spatial structure in the surface chlorophyll field with a relatively low region (~2 mg m^{-3}) west of Ross Bank, moderate values (~5 mg m^{-3}) over the bank, and elevated values in the eastern and western regions of the Ross Sea that approached or exceeded 10 mg m^{-3}.

3.2. Hydrographic survey

The first occupation of the NW-SE section of the bank (Fig. 3, casts 44-37 in Fig. 1) on 20–21 January exhibits a well-defined mixed layer in the upper 30–40 m over the NW part of the transect with temperatures of 0.3–0.7 °C, chlorophyll of 2–5 μg L^{-1}, oxygen of 8.0–8.6 mL L^{-1} and

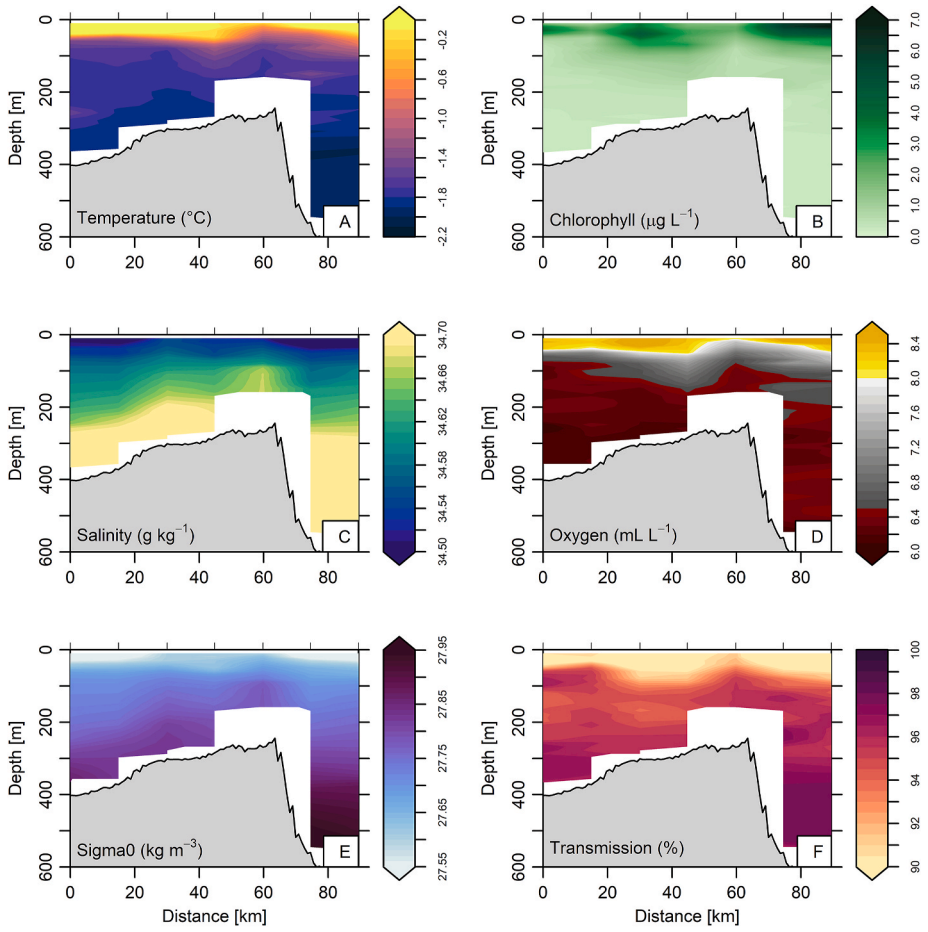

Fig. 3. CTD section of casts 44-37 (NW-SE) prior to the storm event showing (A) conservative temperature, (B) chlorophyll, (C) absolute salinity, (D) dissolved oxygen concentration, (E) seawater density (sigma0) and (F) optical transmission. The tick marks along the top axis of each plot represent the locations of the CTD casts.

light transmission of 87–92%. The station over the crest of the bank was characterized by reduced stratification with lower surface temperature (−0.3 °C), chlorophyll, and oxygen concentrations, along with slight increases in salinity and optical transmission. The off-bank stations to the SE of the crest (casts 37 and 38) show similar vertical structure to that observed over the NW part of this transect with a surface mixed layer temperature of 0–0.2 °C, chlorophyll of 5–7 μg L^{-1}, oxygen of 8.2–8.6 mL L^{-1} and light transmission of 82–87%. These results are very similar to the two other sections occupied during the first hydrographic survey (refer to Figs. S2 and S3), which indicates that there were no substantial temporal changes in ocean properties during the two-day period over which the three sections over Ross Bank were occupied.

The NW-SE section was re-occupied on 26 January (Fig. 4, casts 80-74 in Fig. 1). During the period of 24–25 January, a storm passed over the Ross Bank area and significantly modified the upper ocean properties. The mixed layer deepened to ~75 m, and the area of reduced stratification over the bank had expanded from a small region directly over the crest on the first survey (Fig. 3 Panel E, 25–65 km from start of section) to a horizontal scale extending over most of the bank (Fig. 4 Panel E, 0–65 km from start of section). The surface mixed layer northwest of the Ross Bank crest had cooler temperatures ranging from −0.7 to −0.2 °C with low (relative to the first survey) chlorophyll of ~1 μg L^{-1}, oxygen of 7.5–7.7 mL L^{-1} and high light transmission of 93–94%. Southeast of the bank, surface mixed layer temperature ranged from −0.7 to 0 °C, with chlorophyll of 3–9 μg L^{-1}, oxygen of ~8.1 mL L^{-1} and reduced light transmission of 82–85%.

3.3. Trace metal survey

Profiles of DFe concentration over Ross Bank are consistent with the broader set of observations from the central and western Ross Sea during the NBP12-01 cruise, which showed very low concentrations in the upper 50 m of the water column (average of 0.084 ± 0.074 nM) and increased concentrations with depth (Marsay et al., 2014, 2017). The DFe profiles for the four casts on Ross Bank (TM27, TM28, TM29 and TM37) are similar, with near constant concentrations of ~0.2 nM in the bottom 50–100 m of the water column (Fig. 5). For the two off-bank stations (TM26 and TM30), the DFe concentrations increase with depth, but this increase is more rapid below 400 m and reaches values of approximately 0.7 nM near the seafloor.

3.4. Ross Bank mooring and model simulation

As mentioned in Section 3.2, during the deployment of the SeaHorse mooring near the crest of Ross Bank, a storm transited through the region on 24–25 January. The wind speed at the location of the SeaHorse mooring derived from the ERA-Interim reanalysis (Dee et al., 2011), used to force the ROMS model, ranged from 42 to 97% (average 77%) of the speed measured on the ship (Fig. 6, Panel A). It should be noted that the ship conducted a survey near the Ross Ice Shelf south of Ross Bank during 23–25 January, therefore, the wind data during this period were not co-located with the SeaHorse mooring. However, the ERA-Interim resolution is ~80 km, so it is unlikely that the model wind is much different between the two locations.

A comparison of the SeaHorse CTD data with the ROMS model

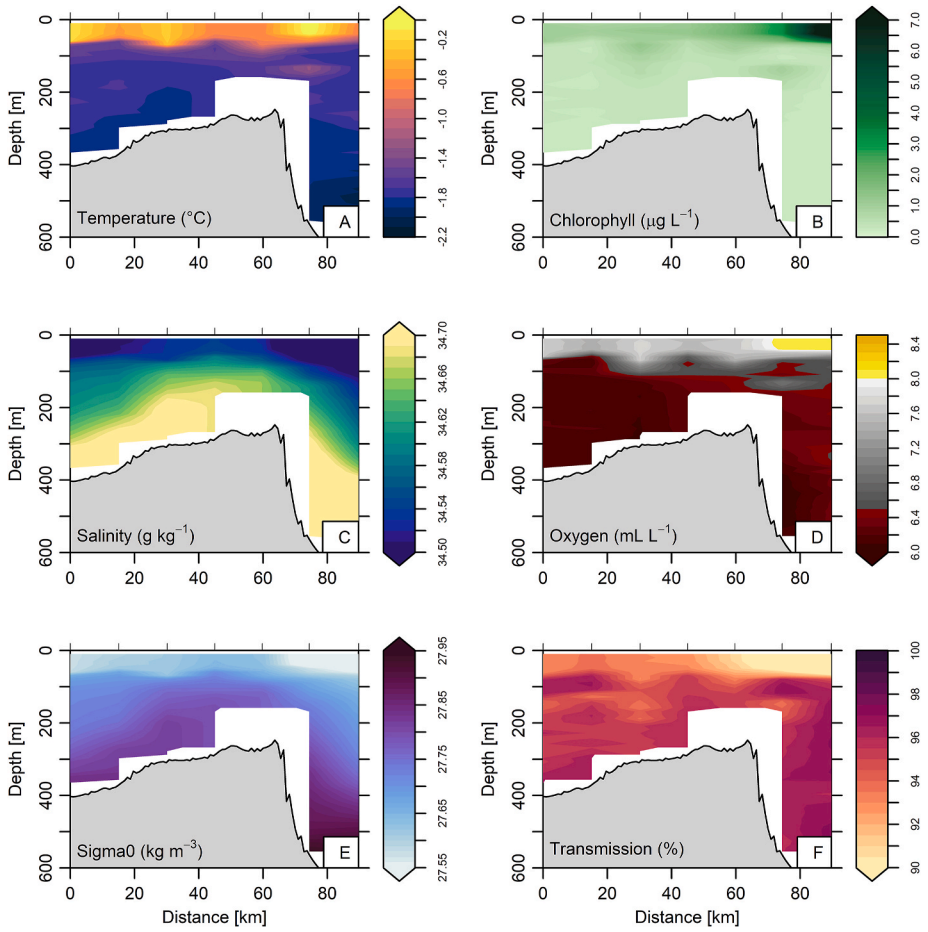

Fig. 4. Same as Fig. 3 for casts 80-74 (NW-SE) acquired after the storm event.

simulation shows that the water temperature at depth is similar in both the mooring record and the model (Fig. 6, Panels B and C); however, in the upper 25 m of the water column, the model is consistently warmer than observations. In this comparison, the SeaHorse mooring provided a profile of the water column every hour, and the ROMS simulation provided output at the model grid point nearest the mooring every 15 min. While the range of salinity in the model simulation (34.40–34.71) is similar to that of the mooring CTD (34.25–34.55), there was an offset in the values (Fig. 6, Panels D and E). The salinity values obtained with the SeaHorse mooring CTD were similar to the results obtained from the shipboard CTD system, which implies that the model salinity was about 0.15 higher than observations throughout the water column.

The surface mixed layer depth was estimated from both the mooring data and model results using a density change criterion of 0.03 kg m^{-3} (Dong et al., 2008), and is represented by the white lines in the bottom two panels of Fig. 6. Both the model and observed data show a deepening of the mixed layer in the latter half of the deployment when the wind forcing increased; however, the model change is much more limited than that observed with the mooring. In general, the mixed layer depth estimated from the SeaHorse mooring is deeper than the ROMS simulation by several tens of meters. There is also significant variability in the observed mixed layer depth with changes of 20–30 m occurring over the period of one day or less, which is not present in the model simulation.

The weak density stratification in the Ross Sea results in circulation on the continental shelf that is strongly forced by the bathymetry as a result of potential vorticity constraints. A comparison of the depth-average currents measured by the ADCPs on the SeaHorse mooring with the tidal model (Padman et al., 2002) and the ROMS velocity show the tidal velocities becoming smaller during the mooring deployment with the shift from spring to neap tides (Fig. 7). When comparing the ADCP and tidal model, the east component of velocity matched well, but the ADCP north component appears to be generally shifted to a more southward direction for most of the deployment. This is consistent with the VM-ADCP results from NBP12-01 (Fig. 8), which indicate a sub-tidal flow to the south on the west side of the bank crest. The magnitude of the ROMS velocity is about 50% of the tidal model estimates; this suggests that the ROMS model underestimates the tidal velocity over Ross Bank, which may explain the higher stratification produced by the model (i.e., there is not enough modeled tidal mixing at this location).

Overall, the ROMS and tidal models appear to be producing results that are qualitatively similar to the physical data observations collected by the SeaHorse mooring on Ross Bank, which is encouraging given that the ROMS implementation is a forward model without data assimilation. However, this comparison has highlighted that the ROMS model has higher stratification in the water column over Ross Bank and this has obvious implications for simulating the vertical resupply of DFe.

3.5. *Seasonality of iron supply*

To complement the *in situ* measurements collected on Ross Bank in January 2012, we employed the ROMS model to provide additional insights into the role of physical processes in the seasonal evolution of DFe in this area. As described in Section 2.2, the ocean model included two passive tracer dyes released in the bottom model layer over the continental shelf for locations with a seafloor depth of less than (greater than) 400 m. The temporal and spatial evolution of the tracer dye in the ocean surface layer is presented in Fig. 9 to provide an understanding of

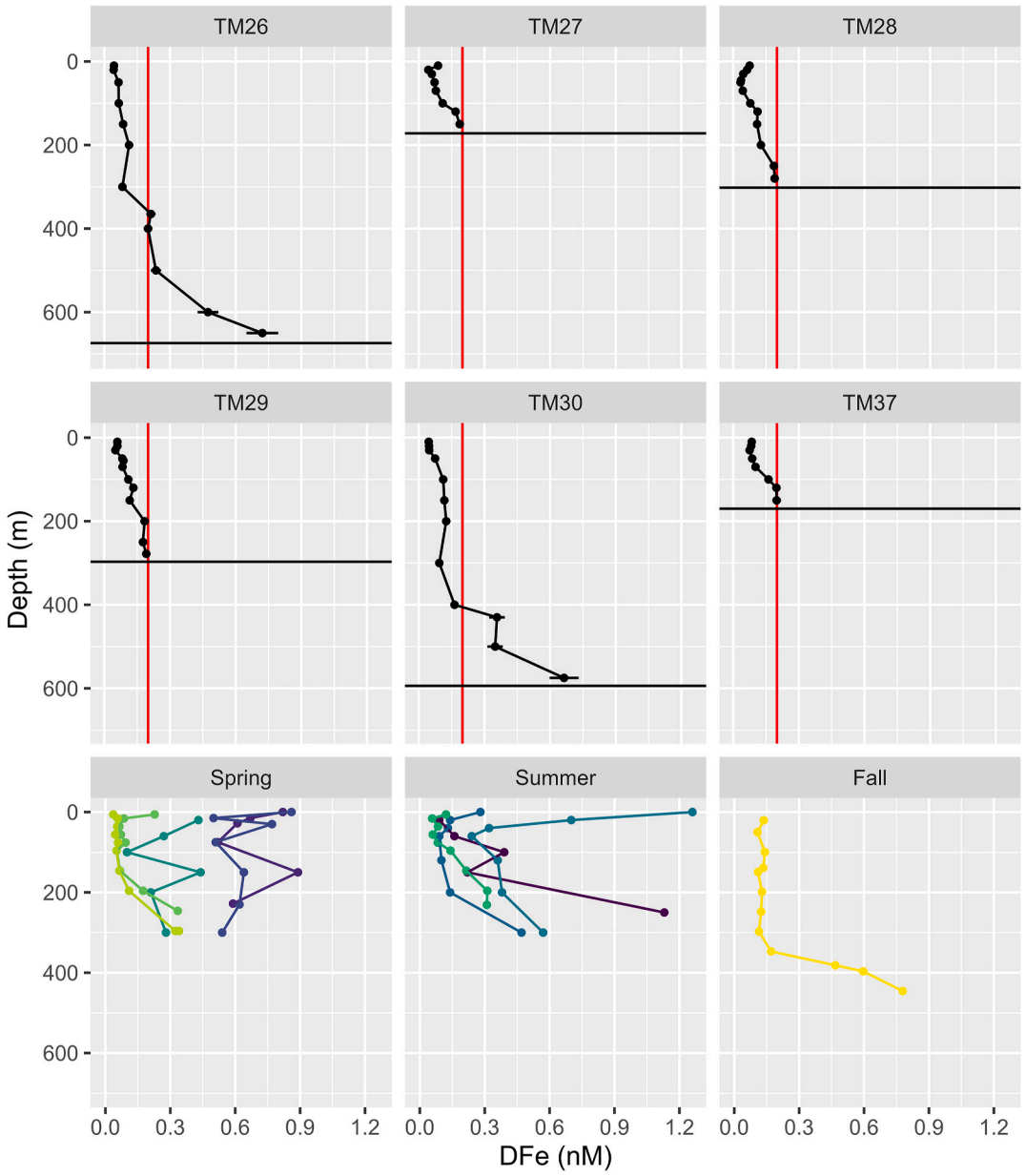

Fig. 5. Dissolved iron concentration as a function of depth. The top two rows are individual casts from NBP12-01 (see Fig. 1 for locations) with casts TM27 and TM37 at the same station collected on the first and second survey of Ross Bank, respectively. The black horizontal line in each plot represents the bottom depth of the station. Error bars (±10%) are shown for the data, but are only evident on the larger DFe values. The red vertical line at DFe = 0.2 nM is provided for a visual reference to assist in comparing profiles. The bottom row represents the historical dFe data collected near Ross Bank grouped by season (Coale et al., 2005; Fitzwater et al., 2000; Sedwick et al., 2000, 2011, 2022). Each historical profile is assigned a unique color. (For interpretation of the references to color in this figure legend, the reader is referred to the Web version of this article.)

the seasonal changes over Ross Bank relative to other areas of the Ross Sea. The end member concentration for the deep locations is approximately four times larger than the shallow regions (1.5 nM vs. 0.4 nM DFe, Section 2.2), so when the tracer dye concentration is scaled to these end members, the relative values are included in the estimate of surface layer DFe concentrations.

In May 2011 (austral fall), the model estimates that DFe in the surface layer from benthic sources is predominantly concentrated in the southern portion of the Ross Sea shelf (Fig. 9). Ross Bank distinguishes itself with an enhanced surface layer DFe mostly derived (up to 80%) from shallow benthic sources over the bank. The other areas showing a high percentage of shallow source iron at this time of year are generally located near the coast. During the austral winter period (represented by the month of July 2011), elevated surface layer DFe expands northward (including over Pennell Bank), as well as under the Ross Ice Shelf. The relative contribution of shallow benthic DFe to total benthic iron in the surface layer over Ross Bank decreased from about 80% to 50% during the two months since May. By September 2011, the extent of enhanced surface concentration has expanded in the Ross Bank area, albeit with somewhat lower values than observed in May (0.75 vs. 1.25 nM), and the trend of the increasing influence of the deep DFe source continues, with it now comprising the majority of the contribution to the surface layer. At this point, the surface layer of most of the Ross Sea has some DFe tracer dye present, as a result of horizontal advection, mixing and diffusion, but at lesser concentrations than over Ross Bank. The spring period (November 2011) is characterized by a surface increase of DFe concentration in the western Ross Sea derived from a combination of shallow and deep sources, but a reduction to ~0.3 nM over Ross Bank,

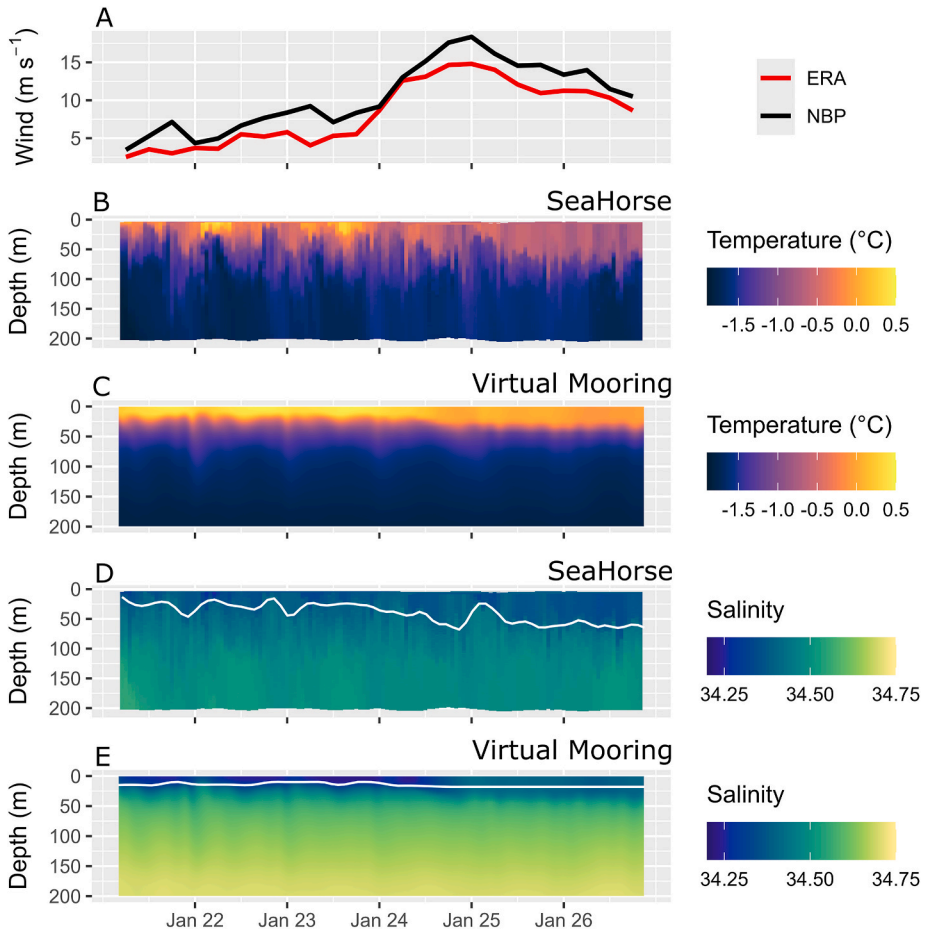

Fig. 6. Wind speed measured by the RVIB NBP and estimated from the ERA-Interim reanalysis during the period of the Ross Bank mooring deployment (Panel A). Temperature and salinity are presented as measured by the SeaHorse CTD (Panel B &D) and from a virtual mooring in the model (Panel C & E). The white lines in the salinity panels represents the mixed layer depth estimated from the density profiles using the criterion of 0.03 kg m^{-3} change relative to the 0–20 m average density (Dong et al., 2008).

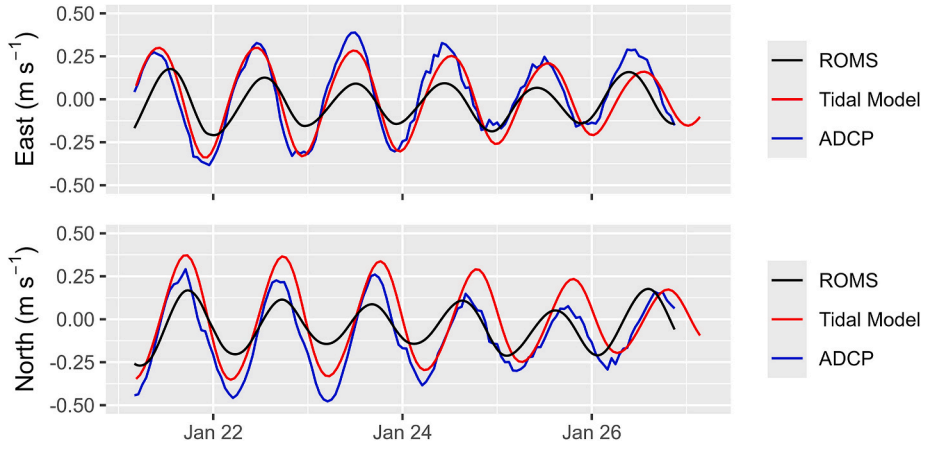

Fig. 7. East and north components of the depth-averaged velocity at the mooring site as measured by ADCPs (blue line) and estimated from the tidal model (red line) and the ROMS model (black line). (For interpretation of the references to color in this figure legend, the reader is referred to the Web version of this article.)

with little change throughout the remainder of the Ross Sea. At this time, the source of DFe in the surface layer over Ross Bank is now almost completely from areas deeper than 400 m, which have been advected on to the bank. In January 2012, the enhanced stratification of the upper ocean in summer (Porter et al., 2019) serves to reduce vertical mixing and the surface layer DFe concentrations, which decreased in all regions relative to November. However, benthic-derived DFe in the surface layer remains elevated over the banks where tidal velocities are large, indicating that these bathymetric features remain as a potential source to surface waters during the mid-summer growing season where vertical mixing, while likely reduced relative to other seasons, still plays a role in vertical transport of DFe.

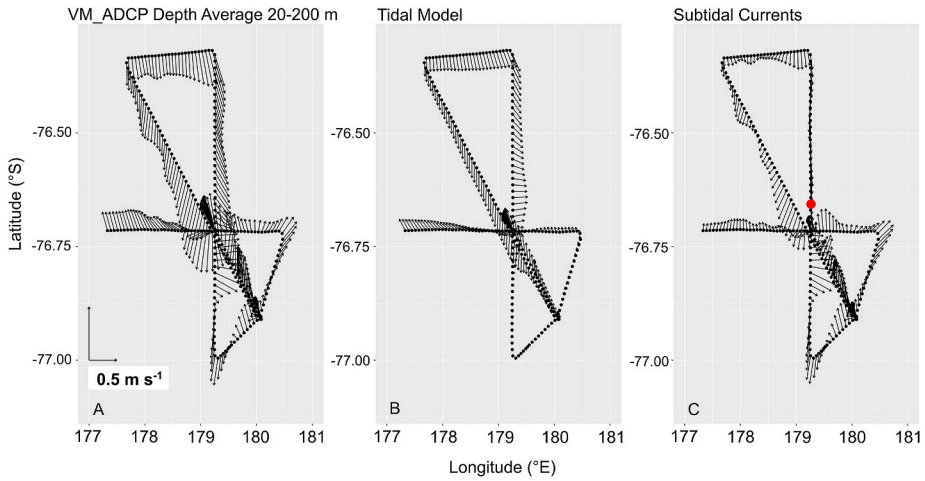

Fig. 8. Vessel-mounted ADCP measurements of depth-averaged (20–200m) currents collected over Ross Bank during 18–21 January 2012 (Panel A), tidal model estimates (Panel B) and subtidal currents calculated as the difference between to VM-ADCP and model results (Panel C). The red dot in Panel C represents the location of the SeaHorse mooring. Scale bar is located in the lower left corner of the panel in the left. The tidal model results are computed using the TMD 2.5 toolbox (https://www.esr.org/research/polar-tide-models/tmd-software/) (Padman et al., 2002).

The simulated temporal evolution of the DFe supply at the location of the SeaHorse mooring near the crest of Ross Bank shows that winter mixing of the water column brings benthic iron from the seafloor of the bank to the surface, and this local source is predominant until July (Fig. 10). The surface water experiences the highest concentrations of benthic-derived DFe in the austral spring period, with both the shallow and deep sources contributing approximately equally. As upper ocean stratification increases in the summer, the vertical DFe supply to the surface layer decreases and is mostly supplied by deep benthic sources. The importance of the higher end member iron concentration in the deep benthic source is evident in the lower part of the water column in the spring and summer period.

To further demonstrate the relative contributions of the shallow and deep benthic DFe sources over Ross Bank, monthly North-South cross-sections of the modeled tracer dye concentrations demonstrate that during May 2011, strong vertical mixing over the crest of Ross Bank results in a uniform concentration of shallow benthic DFe throughout the water column (Fig. 11). For the deep benthic DFe source, there is also vertical mixing on the south side of Ross Bank that reaches the ocean surface, albeit in a lesser concentration compared to the crest of the bank. There is also an indication of a small contribution of deep benthic DFe being advected from the north side of the bank near the seafloor. The ratio of the shallow to total benthic DFe sources indicates that the supply of iron to the surface is principally from the shallow source during late fall. Two months later (July 2011), the shallow benthic source remains important over the crest of the bank but this DFe has propagated both to the south and north. There is also a low but increasing contribution of deep benthic DFe over the bank, as evidenced in the reduction of the ratio of shallow to total benthic DFe to the range of 0.5–0.7. The September cross-section shows a change in the vertical structure of the shallow benthic source over the crest, with the strong gradient now evident between the surface and seafloor. While there does remain an area on the north end of the cross-section that is well-mixed and dominated by shallow benthic DFe, it does not appear that this was advected from the crest of the bank, based on the structure of the tracer dye field from August (not shown). The ratio of shallow to total benthic DFe continues to decrease over the bank.

Increased stratification of the upper ocean is apparent in both the shallow and deep benthic-derived DFe sections for the month of November (Fig. 11). Strong vertical gradients indicate that the vertical transport of benthic sources of iron is much more limited during this period, when the spring phytoplankton bloom typically occurs. Because the ROMS circulation model does not simulate any biological or chemical processes, the low value of iron in the upper water column in the austral summer period is likely attributable to both a reduction in vertical supply along with horizontal advection, mixing and diffusion to areas away from the bank (Fig. 9). Over the bank, there is (in the mean) advection in the surface layer that reduces the surface concentration year round (Mack et al., 2017), but this is most noticeable in the summer, when the vertical supply is reduced. Based on the higher end member concentration of the deep benthic DFe source, the ratio of shallow to total benthic DFe is now dominated by the deep source both on- and off-bank. The January section demonstrates a further reduction in the upper ocean iron concentration during the stratified summer period, and an increased importance of the deep benthic source for the supply of DFe to the upper water column.

A comparison of the January monthly mean DFe tracer dye results from the model (Fig. 11) with the DFe measurements taken by the ship (Fig. 5) reveals a very similar vertical structure for the on-bank stations, with DFe concentrations gradually increasing with depth until they reached a near-constant value in the bottom boundary layer. For the off-bank locations, both the measured and modeled DFe concentrations increased with depth, and this gradient was enhanced below 400 m. In the upper water column, the off-bank iron concentrations were lower than for on-bank locations at the same depth, in both the measured and modeled results. There is also no evidence in the observations of a constant concentration near the seabed at the two stations with water depths around 600 m. This is consistent with the model results which show less evidence of a well-mixed bottom boundary layer in the off-bank area (Fig. 11).

4. Discussion

The hydrographic surveys of Ross Bank before (Fig. 3) and after (Fig. 4) the storm that passed through the region on 24–25 January 2012 indicate that the vertical mixing driven by the event did not supply enough additional nutrients to maintain nor enhance the chlorophyll concentrations observed in the first survey. The column-integrated chlorophyll over the bank was reduced to 30–40% of the value prior to the storm. There were sufficient macronutrients (e.g., phosphate >1 μM, Figs. S4–S7) and light (1% surface PAR value at 30–50 m depth) in the euphotic zone for phytoplankton growth to occur, but it did not. One possibility for the reduction in chlorophyll concentrations is that low-chlorophyll water was advected over Ross Bank by the storm, during which the direction of the strongest winds were from the South-Southeast. A second alternative is that the storm did mix up DFe, but

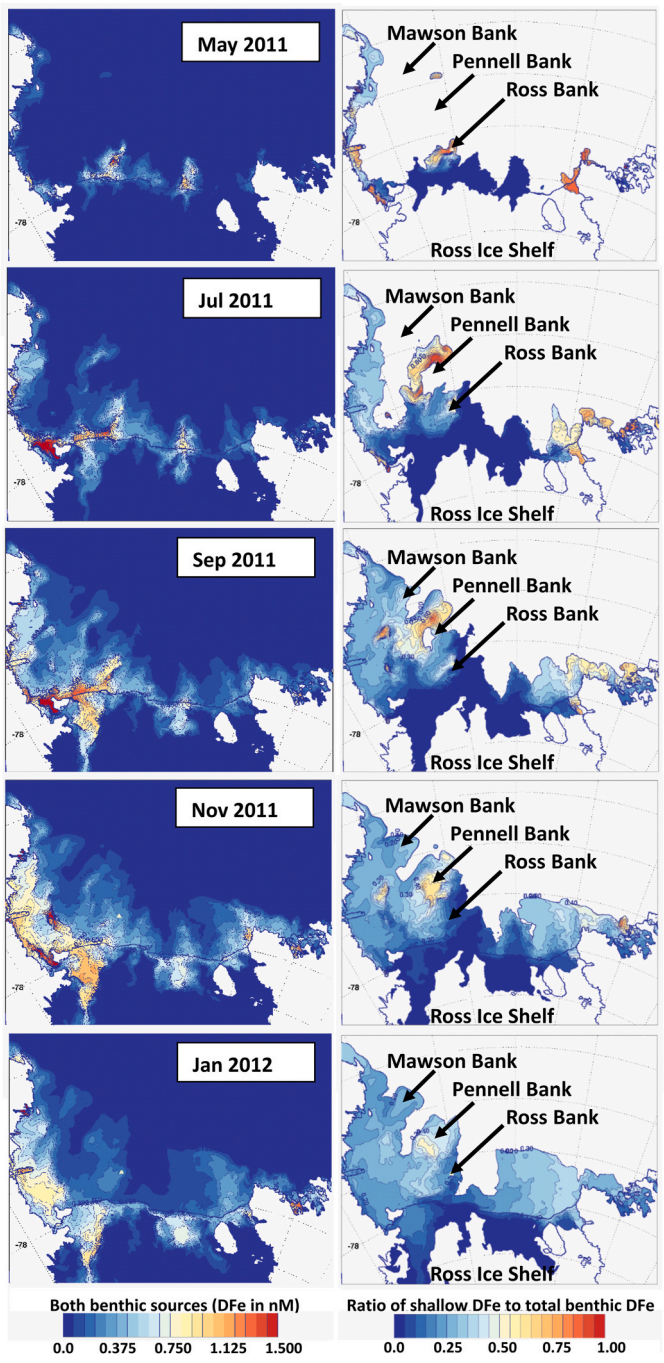

Fig. 9. Model surface layer DFe concentration using end member concentrations from shallow and deep benthic sources (left column). The ratio of shallow to total benthic DFe concentration using the estimated iron end members (right column) where the DFe concentration exceeds a lower threshold of 0.075 nM. Values below the threshold are set to white. The rows represent the monthly average for May, July, September and November 2011, and for January 2012.

the corresponding biological response was incomplete by the time the second survey was finished; however, as shown in Fig. 5, there is little evidence in the DFe results to support this premise. Phytoplankton incubation experiments conducted using samples collected at Ross Bank on NBP12-01 before the storm event showed no significant response to iron addition (Ryan-Keogh et al., 2017), which suggests that this shallow bank may provide continuous DFe inputs to the euphotic zone. Hence, the vertical mixing generated by this storm may not have had a significant short-term impact on the phytoplankton community.

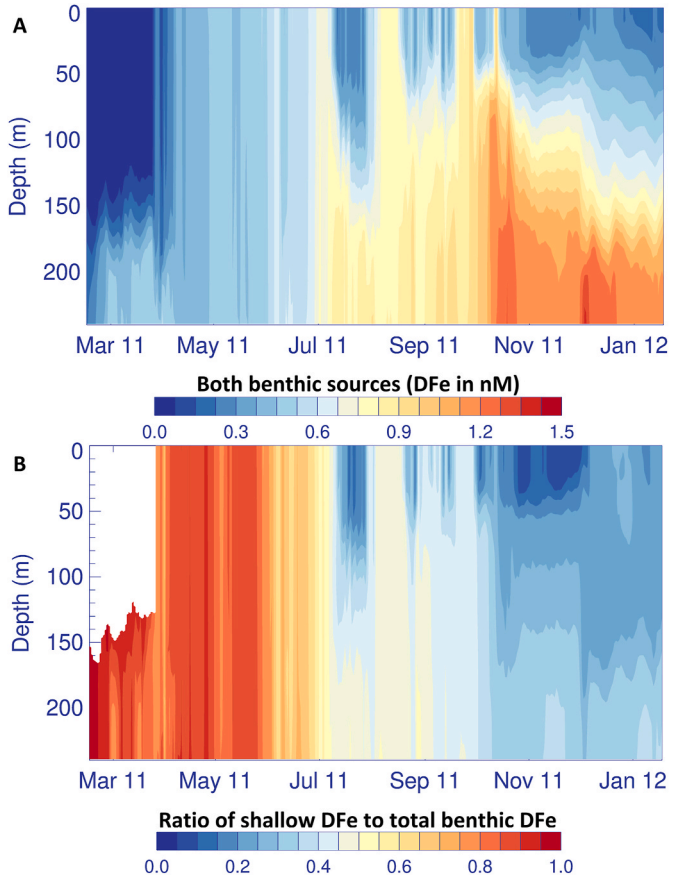

Fig. 10. A) The water column DFe concentration from the ROMS model at the grid point location of the SeaHorse mooring. B) The ratio of shallow to total benthic DFe concentration using the estimated iron end members where the DFe concentration exceeds a lower threshold of 0.075 nM. The white area on the upper left of panel B is below the cutoff threshold.

Based on the PRISM-RS data collected in the central and western Ross Sea, the average mixed layer salinities over Ross Bank (34.19–34.39) were among the highest observed in the region where the values ranged from 32.82 to 34.39 (see Tabl 1, Marsay et al., 2017). The storm event (24–25 January) resulted in a deepening and cooling of the mixed layer as a result of heat loss at the surface (air temperature measured on the ship was as low as −12 °C) and entrainment of cooler water from below (Fig. 6). There was a slight increase in the salinity of the mixed layer in the NW part of the CTD section as a result of the storm event. The off-bank SE station (casts 37, 74) shows a shift to a cooler, fresher mixed layer after the storm event, which likely did not result from local forcing (Fig. 4). While it is not evident in the CTD section plots presented here, benthic nepheloid layers were observed in the transmissometer data near the seafloor in the deep CTD casts to the southeast (casts 37, 74) and east (cast 51) of Ross bank (see Fig. S1, McGillicuddy et al., 2015). The correlation between elevated DFe concentrations and benthic nepheloid layers at NBP12-01 deep stations has been previously documented (Marsay et al., 2014).

To provide baseline context for the DFe profiles collected on Ross Bank during NBP12-01, a summary of the available historical data from this area was compiled and grouped by season (Fig. 5). This historical data does include some substantially higher values in the upper water column in the spring (mostly) and summer. Those higher values have previously been attributed to sea ice meltwater inputs and/or deep convective mixing (e.g., Fitzwater et al., 2000; Sedwick et al., 2000), both of which are expected to be more important early in the growing season, rather than during the late summer NBP12-01 sampling period at Ross Bank where the profiles are similar to the historical fall example.

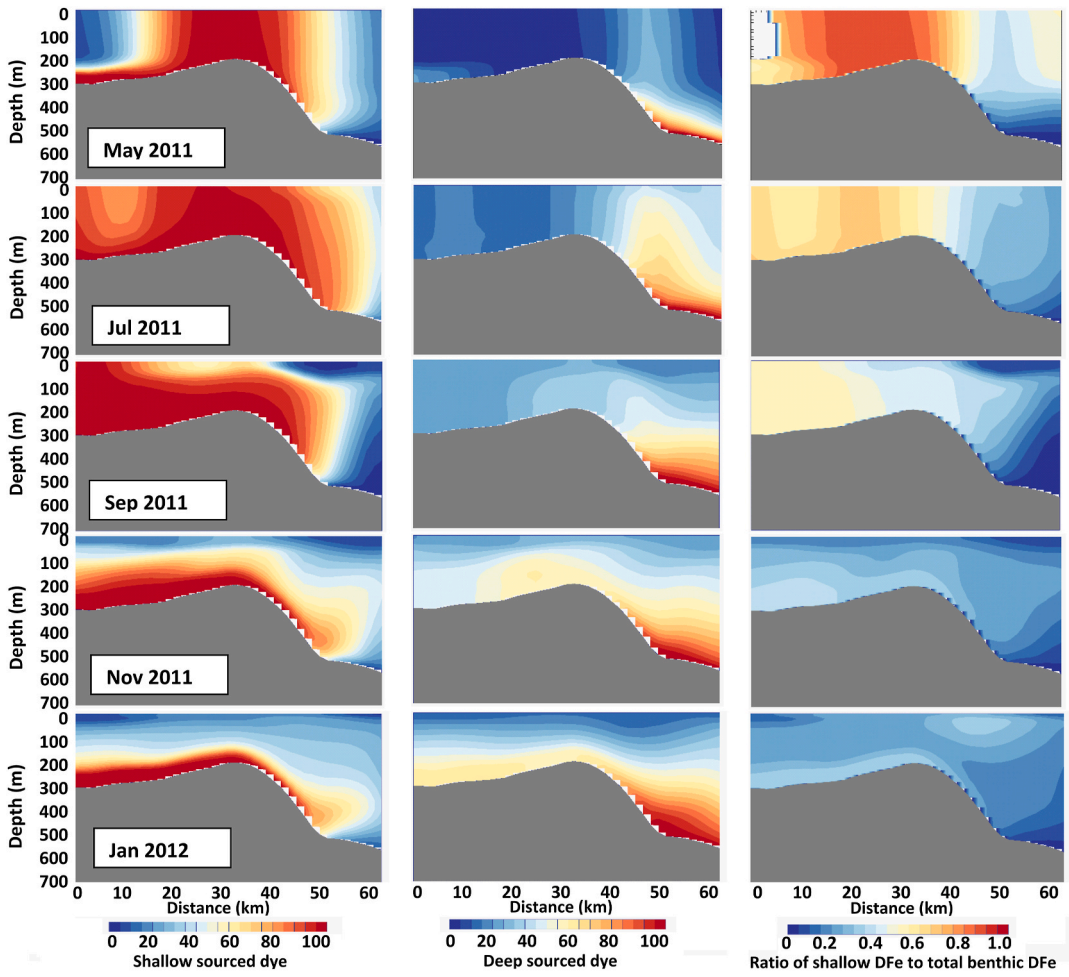

Fig. 11. Model monthly average North-South cross sections over Ross Bank of shallow sourced dye (left column), deep sourced dye (middle column), and ratio of shallow DFe to total benthic DFe (right column) for locations where surface DFe is at least 0.075, assuming end member values of 0.4 nM (shallow source) and 1.5 nM (deep source). The rows represent the monthly average for May, July, September and November 2011, and for January 2012.

As a first approximation, fine sediments and organic matter sinking from the surface (both likely DFe sources) might be expected to be washed off ridges and banks by the large tidal velocities and, therefore, accumulate in topographic depressions (Puig et al., 2014). As indicated above, deep CTD casts indicated the presence of benthic nepheloid layers which typically contain fine sediments, organic matter, and other materials that have been resuspended from the seabed (Anderson et al., 1984; Dunbar et al., 1985). The large increase in DFe concentration observed near the seabed in these off-bank locations (deeper than 400 m) is likely related to the release of DFe from sediment pore waters and resuspended benthic material (Gerringa et al., 2015; Marsay et al., 2014, 2017; McGillicuddy et al., 2015; Sedwick et al., 2011).

The analysis presented in this study of the relative roles of shallow and deep benthic sources in supplying DFe to the upper ocean over Ross Bank is based on both *in situ* physical and chemical observations and simulations from a regional ocean model. An evaluation of the model output vs. observations in January 2012 provides confidence that the model simulations produce a sufficiently accurate representation of the ocean conditions to make credible estimates of benthic DFe supply to surface waters. The model results and SeaHorse mooring data comparison did show that the modeled salinity was higher than observed, and the modeled upper ocean temperature was warmer than observed, resulting in a greater stratification and a shallower surface mixed layer in the model simulations. This indicates that the model may underestimate the vertical transport of iron. However, the overall comparison of the model performance with the SeaHorse mooring data provides confidence in using the ROMS model to explore the seasonal changes in iron supply beyond the time of the NBP12-01 field survey.

As noted in Section 2.2, the ROMS model simulation is limited to the physical processes affecting the supply of benthic DFe to the ocean surface; we do not account for gain or loss of DFe from chemical or biological processes. One example of how this could impact results is that by disregarding biological uptake processes, we underestimate the supply of DFe, because a smaller vertical gradient of DFe concentration is expected to decrease of the amount transported to the euphotic zone via turbulent diffusion. Surface DFe measurements (Fig. 5) were all below 0.1 nM, consistent with other measurements in the Ross Sea during summer (Sedwick et al., 2011), which are thought to reflect biological removal. Moreover, estimates of particle scavenging and subsurface regeneration of DFe (Tagliabue et al., 2019) are also not considered in the model.

An additional caveat about the model is that we have represented benthic dFe inputs by maintaining a fixed concentration of the tracer dye in the bottom layer of the model throughout the run. This implies that the loss of DFe from the bottom boundary layer through mixing, diffusion and advection is balanced by inputs from the sediments/benthic boundary layer. We acknowledge that this is a simplistic approach to modeling the benthic DFe inputs. However, the objective of our analysis is to attempt to improve our understanding of the relative importance of shallow and deep benthic sources in supplying DFe to the ocean surface layer to support primary productivity, rather than focus on the benthic input processes. If the temporal balance of loss and gain processes for

benthic DFe is significantly different for the shallow (on-bank) and deep (off-bank) benthic areas, then this will result in some change in the shallow to total benthic DFe ratios that we have presented. However, our general conclusions regarding the importance of shallow versus deep benthic DFe sources are unlikely to change.

The benthic dye is introduced to the ROMS bottom layer in the month prior to March 15, 2011, at which time it is fully set. Our analysis of the surface layer tracer dye concentrations following this indicates that DFe is initially sourced predominantly from the local benthic layer on Ross Bank, due to the fact that vertical mixing penetrates directly into that layer (Fig. 11). As time progresses through the year, deep DFe is advected on to the bank and eventually becomes the dominant source for the surface layer, in part because of the higher end member concentration assigned to the deep benthic source. If the deep benthic end-member were assumed to be smaller than 1.5 nM, this would result in a proportional increase in the ratio of shallow to deep benthic DFe over Ross Bank. It is possible that during the austral winter 2011 that there was some remnant deep-source benthic iron in the bottom layer over Ross Bank from the previous season. We do not account for this in our analysis and, therefore, may overestimate the ratio of shallow to total benthic DFe during this period. In order to explore interannual changes of DFe on Ross Bank, a more complex model that includes biological uptake, scavenging and precipitation would be required, as these processes likely play an important role in "re-setting" surface dFe levels at the end of the growing season.

It has been suggested that accumulation and remineralization of organic matter on Ross Sea submarine banks may facilitate the vertical resupply of DFe to the euphotic zone throughout the year (Gerringa et al., 2015; Marsay et al., 2014; McGillicuddy et al., 2015). In addition, vertical DFe fluxes are larger above submarine banks and slopes due to a combination of a smaller distance from the benthic DFe source and enhanced eddy diffusivity (Gerringa et al., 2015). The results of our study indicate that Ross Bank does indeed play an important role in vertical DFe supply, however, the model suggests that primary source for DFe is driven by advection of material from nearby deeper areas. Previous studies have demonstrated that Ross, Pennell and Mawson banks have differing physical mechanisms controlling vertical DFe supply (Gerringa et al., 2015; Kohut et al., 2017; Kustka et al., 2015; Mack et al., 2017) and, therefore, further investigation is needed to determine whether the important role of the deep-source DFe supply for Ross Bank also applies to the other submarine banks in the Ross Sea.

5. Conclusions

Previous studies have proposed that supply of iron to the ocean surface layer in the inner shelf region near the Ross Sea polynya is primarily supported by benthic sources (Gerringa et al., 2015; Mack et al., 2017; McGillicuddy et al., 2015). Our analysis demonstrates the important role of deeper benthic sources to the vertical resupply of DFe to surface waters. This is driven, in part, by benthic DFe concentrations being approximately an order of magnitude higher in deeper areas of the Ross Sea as compared to benthic concentrations over shallow banks (Marsay et al., 2014), implying greater input fluxes in deeper areas. In the case of Ross Bank, the advection of this deep DFe supply on to the shallow bank facilitates an enhancement of vertical resupply, because this is a location where tidal mixing results in a reduction of stratification, as observed in the data collected during our field observations. The ROMS simulation suggests that from July 2011–January 2012, the source of benthic DFe in the upper ocean over Ross Bank is dominated by sources deeper than 400 m, which highlights the potential importance of this deep benthic dFe in supporting the seasonal phytoplankton production. Further, the model results for the larger Ross Sea suggest that while there are temporal differences in the timing of the initiation of benthic DFe supply, the deep benthic sources likely play an important role in supporting seasonal primary production in this region.

CRediT authorship contribution statement

Blair J.W. Greenan: Writing – review & editing, Writing – original draft, Visualization, Methodology, Investigation, Formal analysis, Data curation, Conceptualization. **Michael S. Dinniman:** Writing – review & editing, Writing – original draft, Visualization, Methodology, Investigation, Formal analysis, Data curation, Conceptualization. **Dennis J. McGillicuddy Jr.:** Writing – review & editing, Writing – original draft, Project administration, Methodology, Investigation, Funding acquisition, Formal analysis, Data curation, Conceptualization. **Peter N. Sedwick:** Writing – review & editing, Methodology, Investigation, Funding acquisition, Formal analysis, Data curation, Conceptualization. **Stefanie L. Mack:** Writing – review & editing, Methodology, Investigation, Formal analysis, Data curation. **Walker O. Smith Jr.:** Writing – review & editing, Writing – original draft, Methodology, Investigation, Funding acquisition, Formal analysis, Conceptualization.

Declaration of competing interest

The authors declare that they have no known competing financial interests or personal relationships that could have appeared to influence the work reported in this paper.

Acknowledgments

The authors would like to acknowledge the support of the officers, crew and science team on the RVIB Nathaniel B Palmer cruise NBP12-01. Dr. S. Chen provided the ocean color information. The data used in this paper are archived at the Biological and Chemical Oceanography Data Management Office: www.bco-dmo.org/project/2155. The authors acknowledge funding from National Science Foundation's Antarctic Research Program (ODU: ANT-0944174; WHOI: ANT-0094165; VIMS: ANT-0944254) and Fisheries and Ocean Canada (DFO). Computing support was provided by the Wahab High Performance Computing cluster at Old Dominion University. The authors would also like to acknowledge the comments and suggestions provided by two reviewers, which helped improve this paper.

Appendix A. Supplementary data

Supplementary data to this article can be found online at https://doi.org/10.1016/j.dsr2.2024.105450.

Data availability

The data used in this paper are archived at the Biological and Chemical Oceanography Data Management Office: www.bco-dmo.org/project/2155

References

Anderson, J.B., 1999. Antarctic Marine Geology. Cambridge University Press, Cambridge, U.K.

Anderson, J.B., Brake, C.F., Myers, N.C., 1984. Sedimentation on the Ross Sea continental shelf, Antarctica. Marine Geology, Sedimentation on High-latitude Continental Shelves 57, 295–333. https://doi.org/10.1016/0025-3227(84)90203-2.

Arndt, J.E., Schenke, H.W., Jakobsson, M., Nitsche, F.O., Buys, G., Goleby, B., Rebesco, M., Bohoyo, F., Hong, J., Black, J., Greku, R., Udintsev, G., Barrios, F., Reynoso-Peralta, W., Taisei, M., Wigley, R., 2013. The International bathymetric Chart of the Southern Oceanocean (IBCSO) version 1.0—a new bathymetric compilation covering circum-Antarctic waters. Geophys. Res. Lett. 40, 3111–3117. https://doi.org/10.1002/grl.50413.

Arrigo, K.R., Van Dijken, G.L., Bushinsky, S., 2008. Primary production in the Southern Ocean, 1997–2006. J. Geophys. Res. 113, C08004. https://doi.org/10.1029/2007JC004551.

Arrigo, K.R., Worthen, D., Schnell, A., Lizotte, M.P., 1998. Primary production in Southern Ocean waters. J. Geophys. Res. 103, 15587–15600. https://doi.org/10.1029/98JC00930.

Barry, J.P., Grebmeier, J.M., Smith, J., Dunbar, R.B., 2003. Oceanographic versus seafloor-habitat control of benthic megafaunal communities in the S.W. Ross Sea,

Antarctica. In: DiTullio, G.R., Dunbar, R.B. (Eds.), Antarctic Research Series. American Geophysical Union, pp. 327–353. https://doi.org/10.1029/078ARS21. Washington, D. C.

Bertrand, E.M., Saito, M.A., Rose, J.M., Riesselman, C.R., Lohan, M.C., Noble, A.E., Lee, P.A., DiTullio, G.R., 2007. Vitamin B $_{12}$ and iron colimitation of phytoplankton growth in the Ross Sea. Limnol. Oceanogr. 52, 1079–1093. https://doi.org/10.4319/lo.2007.52.3.1079.

Boyd, P.W., Ellwood, M.J., 2010. The biogeochemical cycle of iron in the ocean. Nature Geosci 3, 675–682. https://doi.org/10.1038/ngeo964.

Boyer, T.P., Garcia, H.E., Locarnini, R.A., Zweng, M.M., Mishonov, A.V., Reagan, J.R., Weathers, K.A., Baranova, O.K., Seidov, D., Smolyar, I.V., 2018. World Ocean Atlas. https://www.ncei.noaa.gov/archive/accession/NCEI-WOA18.

Budgell, W.P., 2005. Numerical simulation of ice-ocean variability in the Barents Sea region: towards dynamical downscaling. Ocean Dynam. 55, 370–387. https://doi.org/10.1007/s10236-005-0008-3.

Castagno, P., Falco, P., Dinniman, M.S., Spezie, G., Budillon, G., 2017. Temporal variability of the circumpolar deep water inflow onto the Ross Sea continental shelf. J. Mar. Syst. 166, 37–49. https://doi.org/10.1016/j.jmarsys.2016.05.006.

Cavalieri, D.J., Parkinson, C.L., Gloersen, P., Zwally, H.J., 1996. Sea Ice Concentrations from Nimbus-7 SMMR and DMSP SSM/I-SSMIS Passive Microwave Data, Version 1. https://doi.org/10.5067/8GQ8LZQVL0VL. (Accessed 2 December 2024).

Chen, S., Smith, W.O., Yu, X., 2021. Revisiting the Ocean color algorithms for particulate organic carbon and chlorophyll-a concentrations in the Ross Sea. J. Geophys. Res. Oceans 126, e2021JC017749. https://doi.org/10.1029/2021JC017749.

Coale, K.H., Michael Gordon, R., Wang, X., 2005. The distribution and behavior of dissolved and particulate iron and zinc in the Ross Sea and Antarctic circumpolar current along 170°W. Deep Sea Res. Oceanogr. Res. Pap. 52, 295–318. https://doi.org/10.1016/j.dsr.2004.09.008.

Coale, K.H., Wang, X., Tanner, S.J., Johnson, K.S., 2003. Phytoplankton growth and biological response to iron and zinc addition in the Ross Sea and Antarctic Circumpolar Current along 170°W. Deep Sea Res. Part II Top. Stud. Oceanogr. 50, 635–653. https://doi.org/10.1016/S0967-0645(02)00588-X.

Dee, D.P., Uppala, S.M., Simmons, A.J., Berrisford, P., Poli, P., Kobayashi, S., Andrae, U., Balmaseda, M.A., Balsamo, G., Bauer, P., Bechtold, P., Beljaars, A.C.M., Van De Berg, L., Bidlot, J., Bormann, N., Delsol, C., Dragani, R., Fuentes, M., Geer, A.J., Haimberger, L., Healy, S.B., Hersbach, H., Hólm, E.V., Isaksen, L., Kållberg, P., Köhler, M., Matricardi, M., McNally, A.P., Monge-Sanz, B.M., Morcrette, J.-J., Park, B.-K., Peubey, C., De Rosnay, P., Tavolato, C., Thépaut, J.-N., Vitart, F., 2011. The ERA-Interim reanalysis: configuration and performance of the data assimilation system. Quart J Royal Meteoro Soc 137, 553–597. https://doi.org/10.1002/qj.828.

Dinniman, M.S., Klinck, J.M., Smith Jr., W.O., 2007. Influence of sea ice cover and icebergs on circulation and water mass formation in a numerical circulation model of the Ross Sea, Antarctica. J. Geophys. Res.: Oceans 112, C11013. https://doi.org/10.1029/2006JC004036. Jr.

Dinniman, M.S., Klinck, J.M., Smith Jr., W.O., 2011. A model study of circumpolar deep water on the west Antarctic Peninsula and Ross Sea continental shelves. Deep Sea Res. Part II Top. Stud. Oceanogr. 58, 1508–1523. https://doi.org/10.1016/j.dsr2.2010.11.013.

Dong, S., Sprintall, J., Gille, S.T., Talley, L., 2008. Southern Ocean mixed-layer depth from Argo float profiles. J. Geophys. Res. 113, C06013. https://doi.org/10.1029/2006JC004051.

Dunbar, R.B., Anderson, J.B., Domack, E.W., Jacobs, S.S., 1985. Oceanographic influences on sedimentation along the Antarctic continental shelf. In: Jacobs, S.S. (Ed.), Oceanology of the Antarctic Continental Shelf. AGU, Washington, D. C., pp. 291–312

Durski, S.M., Glenn, S.M., Haidvogel, D.B., 2004. Vertical mixing schemes in the coastal ocean: comparison of the level 2.5 Mellor-Yamada scheme with an enhanced version of the K profile parameterization. J. Geophys. Res. 109, 2002JC001702. https://doi.org/10.1029/2002JC001702.

Fitch, D.T., Moore, J.K., 2007. Wind speed influence on phytoplankton bloom dynamics in the Southern Ocean marginal ice zone. J. Geophys. Res. 112, C08006. https://doi.org/10.1029/2006JC004061.

Fitzwater, S.E., Johnson, K.S., Gordon, R.M., Coale, K.H., Smith, W.O., 2000. Trace metal concentrations in the Ross Sea and their relationship with nutrients and phytoplankton growth. Deep Sea Research Part II: Topical Studies in Oceanography, US Southern Ocean JGOFS Program (AESOPS) 47, 3159–3179. https://doi.org/10.1016/S0967-0645(00)00063-1.

Fretwell, P., Pritchard, H.D., Vaughan, D.G., Bamber, J.L., Barrand, N.E., Bell, R., Bianchi, C., Bingham, R.G., Blankenship, D.D., Casassa, G., Catania, G., Callens, D., Conway, H., Cook, A.J., Corr, H.F.J., Damaske, D., Damm, V., Ferraccioli, F., Forsberg, R., Fujita, S., Gim, Y., Gogineni, P., Griggs, J.A., Hindmarsh, R.C.A., Holmlund, P., Holt, J.W., Jacobel, R.W., Jenkins, A., Jokat, W., Jordan, T., King, E. C., Kohler, J., Krabill, W., Riger-Kusk, M., Langley, K.A., Leitchenkov, G., Leuschen, C., Luyendyk, B.P., Matsuoka, K., Mouginot, J., Nitsche, F.O., Nogi, Y., Nost, O.A., Popov, S.V., Rignot, E., Rippin, D.M., Rivera, A., Roberts, J., Ross, N., Siegert, M.J., Smith, A.M., Steinhage, D., Studinger, M., Sun, B., Tinto, B.K., Welch, B.C., Wilson, D., Young, D.A., Xiangbin, C., Zirizzotti, A., 2013. Bedmap2: improved ice bed, surface and thickness datasets for Antarctica. Cryosphere 7, 375–393. https://doi.org/10.5194/tc-7-375-2013.

Gerringa, L.J.A., Laan, P., van Dijken, G.L., van Haren, H., De Baar, H.J.W., Arrigo, K.R., Alderkamp, A.-C., 2015. Sources of iron in the Ross Sea polynya in early summer. Mar. Chem. 177, 447–459. https://doi.org/10.1016/j.marchem.2015.06.002.

Greenan, B.J.W., Petrie, B.D., Harrison, W.G., Strain, P.M., 2008. The onset and evolution of a spring bloom on the Scotian Shelf. Limnol. Oceanogr. 53, 1759–1775. https://doi.org/10.4319/lo.2008.53.5.1759.

Haidvogel, D.B., Arango, H., Budgell, W.P., Cornuelle, B.D., Curchitser, E., Lorenzo, E.D., Fennel, K., Geyer, W.R., Hermann, A.J., Lanerolle, L., Levin, J., McWilliams, J.C., Miller, A.J., Moore, A.M., Powell, T.M., Shchepetkin, A.F., Sherwood, C.R., Signell, R.P., Warner, J.C., Wilkin, J., 2008. Ocean forecasting in terrain-following coordinates: Formulation and skill assessment of the regional Ocean modeling system. J. Comput. Phys. 227, 3595–3624. https://doi.org/10.1016/j.jcp.2007.06.016.

Hamilton, J.M., Fowler, G., Beanlands, B., 1999. Long-term monitoring with a moored wave-powered profiler. Sea Technol. 68–69.

Kohut, J., Hunter, E., Huber, B., 2013. Small-scale variability of the cross-shelf flow over the outer shelf of the Ross Sea. J. Geophys. Res. Oceans 118, 1863–1876. https://doi.org/10.1002/jgrc.20090.

Kohut, J.T., Kustka, A.B., R Hiscock, M., Lam, P.J., Measures, C., Milligan, A., White, A., Carvalho, F., Hatta, M., Jones, B.M., Ohnemus, D.C., Swartz, J.M., 2017. Mesoscale variability of the summer bloom over the northern Ross Sea shelf: a tale of two banks. J. Mar. Syst. 166, 50–60. https://doi.org/10.1016/j.jmarsys.2016.06.009.

Kustka, A.B., Kohut, J.T., White, A.E., Lam, P.J., Milligan, A.J., Dinniman, M.S., Mack, S., Hunter, E., Hiscock, M.R., Smith Jr., W.O., Measures, C.I., 2015. The roles of MCDW and deep water iron supply in sustaining a recurrent phytoplankton bloom on central Pennell Bank (Ross Sea). Deep Sea Res. Oceanogr. Res. Pap. 105, 171–185. https://doi.org/10.1016/j.dsr.2015.08.012.

Large, W.G., McWilliams, J.C., Doney, S.C., 1994. Oceanic vertical mixing: a review and a model with a nonlocal boundary layer parameterization. Rev. Geophys. 32, 363–403. https://doi.org/10.1029/94RG01872.

Mack, S.L., Dinniman, M.S., McGillicuddy, D.J., Sedwick, P.N., Klinck, J.M., 2017. Dissolved iron transport pathways in the Ross Sea: influence of tides and horizontal resolution in a regional ocean model. J. Mar. Syst. 166, 73–86. https://doi.org/10.1016/j.jmarsys.2016.10.008.

Marsay, C.M., Barrett, P.M., McGillicuddy, D.J., Sedwick, P.N., 2017. Distributions, sources, and transformations of dissolved and particulate iron on the Ross Sea continental shelf during summer. J. Geophys. Res. Oceans 122, 6371–6393. https://doi.org/10.1002/2017JC013068.

Marsay, C.M., Sedwick, P.N., Dinniman, M.S., Barrett, P.M., Mack, S.L., McGillicuddy, D. J., 2014. Estimating the benthic efflux of dissolved iron on the Ross Sea continental shelf: benthic dFe flux on the Ross Sea shelf. Geophys. Res. Lett. 41, 7576–7583. https://doi.org/10.1002/2014GL061684.

Martin, J.H., 1990. Glacial-interglacial CO $_{2}$ change: the iron Hypothesis. Paleoceanography 5, 1–13. https://doi.org/10.1029/PA005i001p00001.

Martin, J.H., Gordon, M., Fitzwater, S.E., 1991. The case for iron. Limnol. Oceanogr. 36, 1793–1802. https://doi.org/10.4319/lo.1991.36.8.1793.

McGillicuddy, D.J., Sedwick, P.N., Dinniman, M.S., Arrigo, K.R., Bibby, T.S., Greenan, B. J.W., Hofmann, E.E., Klinck, J.M., Smith, W.O., Mack, S.L., Marsay, C.M., Sohst, B. M., Dijken, G.L., 2015. Iron supply and demand in an Antarctic shelf ecosystem. Geophys. Res. Lett. 42, 8088–8097. https://doi.org/10.1002/2015GL065727.

Measures, C.I., Yuan, J., Resing, J.A., 1995. Determination of iron in seawater by flow injection analysis using in-line preconcentration and spectrophotometric detection. Marine Chemistry, The Chemistry of Iron in Seawater and its Interaction with Phytoplankton 50, 3–12. https://doi.org/10.1016/0304-4203(95)00022-J.

Moore, J.K., Abbott, M.R., 2000. Phytoplankton chlorophyll distributions and primary production in the Southern Ocean. J. Geophys. Res. 105, 28709–28722. https://doi.org/10.1029/1999JC000043.

Padman, L., Fricker, H.A., Coleman, R., Howard, S., Erofeeva, L., 2002. A new tide model for the Antarctic ice shelves and seas. Ann. Glaciol. 34, 247–254. https://doi.org/10.3189/172756402781817752.

Porter, D.F., Springer, S.R., Padman, L., Fricker, H.A., Tinto, K.J., Riser, S.C., Bell, R.E., the ROSETTA-Ice Team, 2019. Evolution of the seasonal surface mixed layer of the Ross Sea, Antarctica, observed with Autonomous profiling Floats. J. Geophys. Res. Oceans 124, 4934–4953. https://doi.org/10.1029/2018JC014683.

Powers, J.G., Monaghan, A.J., Cayette, A.M., Bromwich, D.H., Kuo, Y.-H., Manning, K. W., 2003. Real-time Mesoscale modeling over Antarctica: the Antarctic Mesoscale Prediction system. Bull. Am. Meteorol. Soc. 84, 1533–1546. https://doi.org/10.1175/BAMS-84-11-1533.

Puig, P., Palanques, A., Martín, J., 2014. Contemporary sediment-transport processes in submarine Canyons. Ann. Rev. Mar. Sci 6, 53–77. https://doi.org/10.1146/annurev-marine-010213-135037.

Rossow, W.B., Walker, A.W., Beuschel, D.E., Roiter, M.D., 1996. International Satellite Cloud Climatology Project (ISCCP): Documentation of New Cloud Datasets (No. WMO/TD-737). World Meteorological Organization.

Ryan-Keogh, T.J., DeLizo, L.M., Smith, W.O., Sedwick, P.N., McGillicuddy, D.J., Moore, C.M., Bibby, T.S., 2017. Temporal progression of photosynthetic-strategy in phytoplankton in the Ross Sea, Antarctica. J. Mar. Syst. 166, 87–96. https://doi.org/10.1016/j.jmarsys.2016.08.014.

Salmon, E., Hofmann, E.E., Dinniman, M.S., Smith, W.O., 2020. Evaluation of iron sources in the Ross Sea. J. Mar. Syst. 212, 103429. https://doi.org/10.1016/j.jmarsys.2020.103429.

Saunders, P.M., Coward, A.C., De Cuevas, B.A., 1999. Circulation of the Pacific ocean seen in a global ocean model: ocean Circulation and climate Advanced Modelling project (OCCAM). J. Geophys. Res. 104, 18281–18299. https://doi.org/10.1029/1999JC900091.

Sedwick, P.N., DiTullio, G.R., 1997. Regulation of algal blooms in Antarctic Shelf Waters by the release of iron from melting sea ice. Geophys. Res. Lett. 24, 2515–2518. https://doi.org/10.1029/97GL02596.

Sedwick, P.N., DiTullio, G.R., Mackey, D.J., 2000. Iron and manganese in the Ross Sea, Antarctica: seasonal iron limitation in Antarctic shelf waters. J. Geophys. Res. 105, 11321–11336. https://doi.org/10.1029/2000JC000256.

Sedwick, P.N., Marsay, C.M., Sohst, B.M., Aguilar-Islas, A.M., Lohan, M.C., Long, M.C., Arrigo, K.R., Dunbar, R.B., Saito, M.A., Smith, W.O., DiTullio, G.R., 2011. Early season depletion of dissolved iron in the Ross Sea polynya: implications for iron dynamics on the Antarctic continental shelf. J. Geophys. Res. 116, C12019. https://doi.org/10.1029/2010JC006553.

Sedwick, P.N., Sohst, B.M., O'Hara, C., Stammerjohn, S.E., Loose, B., Dinniman, M.S., Buck, N.J., Resing, J.A., Ackley, S.F., 2022. Seasonal dynamics of dissolved iron on the Antarctic continental shelf: late-fall observations from the Terra Nova Bay and Ross ice shelf polynyas. J. Geophys. Res. Oceans 127. https://doi.org/10.1029/2022JC018999.

Shchepetkin, A.F., McWilliams, J.C., 2009. Correction and commentary for "Ocean forecasting in terrain-following coordinates: Formulation and skill assessment of the regional ocean modeling system" by Haidvogel et al. J. Comp. Phys. 227, 3595–3624. https://doi.org/10.1016/j.jcp.2009.09.002. Journal of Computational Physics 228, 8985–9000.

Shchepetkin, A.F., McWilliams, J.C., 2005. The regional oceanic modeling system (ROMS): a split-explicit, free-surface, topography-following-coordinate oceanic model. Ocean Model. 9, 347–404. https://doi.org/10.1016/j.ocemod.2004.08.002.

Smith Jr., W.O., Ainley, D.G., Arrigo, K.R., Dinniman, M.S., 2014. The oceanography and Ecology of the Ross Sea. Annu. Rev. Mar. Sci. 6, 469–487. https://doi.org/10.1146/annurev-marine-010213-135114.

Smith Jr., W.O., Kaufman, D.E., 2018. Climatological temporal and spatial distributions of nutrients and particulate matter in the Ross Sea. Prog. Oceanogr. 168, 182–195. https://doi.org/10.1016/j.pocean.2018.10.003.

Smith, W.O., Shields, A.R., Peloquin, J.A., Catalano, G., Tozzi, S., Dinniman, M.S., Asper, V.A., 2006. Interannual variations in nutrients, net community production, and biogeochemical cycles in the Ross Sea. Deep Sea Research Part II: Topical Studies in Oceanography, EASIZ: Ecology of the Antarctic Sea Ice Zone 53, 815–833. https://doi.org/10.1016/j.dsr2.2006.02.014.

Song, Y., Haidvogel, D., 1994. A Semi-implicit Ocean Circulation model using a Generalized topography-following coordinate system. J. Comput. Phys. 115, 228–244. https://doi.org/10.1006/jcph.1994.1189.

Tagliabue, A., Bowie, A.R., DeVries, T., Ellwood, M.J., Landing, W.M., Milne, A., Ohnemus, D.C., Twining, B.S., Boyd, P.W., 2019. The interplay between regeneration and scavenging fluxes drives ocean iron cycling. Nat. Commun. 10, 4960. https://doi.org/10.1038/s41467-019-12775-5.